Separation patterns between Brazilian nut and reversed Brazilian nut of a binary granular system

Zi-Ang Xie,[1] Ping Wu,[1,*] Shi-Ping Zhang,[1] Sen Chen,[1] Chao Jia,[2] Chuan-Ping Liu,[2] and Li Wang[2]
[1]*School of Mathematics and Physics, University of Science and Technology Beijing, Beijing 100083, China*
[2]*School of Mechanical Engineering, University of Science and Technology Beijing, Beijing 100083, China*
(Received 8 February 2012; published 4 June 2012)

This paper studies the segregation behavior of binary granular particles with diameters at approximately 10:1 in a vertically vibrated container. An array of transitional separation patterns between reversed Brazilian nut (RBN) and Brazilian nut (BN) separations are observed, with their geometrical features carefully measured. The binary particle system develops into either a stable separation pattern when f and Γ are relatively low or an oscillating pattern when f and Γ are relatively high. We regard these patterns as different phases, in which the stable patterns can be divided into phases of RBN, RBN transitional (RBNT), BNT, and BN. A phase parameter λ between -1 and 1 is defined to describe the separation patterns based on the mass center height difference in large and small particles. By drawing f-Γ-λ phase diagrams, the system's tendency toward BN separation was found to increase with f and decrease with Γ. Furthermore, the range of the tendency toward BN separation expands when the size of small particles rises. As the total mass of the small particles increases, the system's tendency toward RBN separation is enhanced. Abnormal points are also observed in the stable phase regions, and the oscillating phase shifts among the four stable phases with time. These stable phases can be explained via an analysis of the distribution of the dissipation energy, whereas the mechanism of the oscillating phase remains to be discovered.

DOI: 10.1103/PhysRevE.85.061302 PACS number(s): 45.70.Mg, 05.65.+b, 45.70.Vn

I. INTRODUCTION

Granular particles of different sizes in a container can be separated by exerting vertical vibrations on the particle system, and the separation pattern differs significantly because of vibration parameters. Under certain vibration parameters, an extremely common yet important phenomenon, Brazilian nut (BN) separation, occurs when large particles rise to the top and small ones sink to the bottom [1]. Contrary to the BN mode, when small particles gain height and cover the large ones, a reversed Brazilian nut (RBN) separation [2] occurs. In previous studies, other patterns, such as sandwich separation [3], in which the small particles form a layer in the middle and the entire structure remains stable, were also reported. Numerous researchers regard these separation phases differently and attempt to discover the physical mechanism of these separation results [4–7]. However, a complete understanding of the entire process of separation and segregation patterns is needed [8–10].

To understand these phenomena fully, one important method is to study and compare the effects of the vibration and system parameters on the final separation result. These factors include vibration frequency f, amplitude A, dimensionless acceleration $\Gamma = A\omega^2/g$, total mass ratio μ_m, and diameter ratio μ_φ of the binary particles, as well as the coefficients of friction and elasticity and so on [10]. The majority of the performed experiments each studied a certain factor. However, the other settings may also be diverse, and difficulty arises in the analytical comparison based on the "one variable" credits. As a result, experimental findings can be controversial. For example, a rising f may result in better BN separation [11] or, under other conditions, an RBN separation result [12]. Shishidia demonstrated that a greater A brings BN separation [13], whereas Burtally proved the opposite [14]. An increase in diameter ratio was also found to be in favor of BN [11] or RBN [15] separation. Such contradictory situations have resulted in a great deal of confusion, and an overall method of research is needed for in-depth development. Accordingly, a technique for scanning phase diagrams was proposed. Shi sketched two-dimensional f-Γ phase diagrams, in which BN, RBN, and the sandwich phase regions were clearly exhibited and divided [16]. Zhao formatted a three-dimensional (3D) phase diagram containing 16 data points to enhance this method further [17].

In our research, the formative process and final structure of the separation pattern under different vibration parameters were carefully studied via the phase diagram method. A phase parameter λ associated with the difference in mass center height of the large and small particles was defined to describe the separation patterns. Six 3D f-Γ-λ phase diagrams (each containing approximately 400 sampled points) were plotted to study the effect of the frequency f, dimensionless acceleration Γ, total mass ratio μ_m, and diameter ratio μ_φ of binary particles on the final separation results, thus providing a significantly clearer view of the general tendencies when parameters change. Essentially, f and Γ are external vibration parameters, whereas μ_m and μ_φ are parameters of the granular system. Discussions regarding the separation mechanisms were also conducted, delving further into the final separation patterns and dissipative energy distributions of the large and small particles.

II. EXPERIMENT

A. Basic settings

As shown in Fig. 1, an LDS Daction standard vibrating system was applied in our experiments. The LDS-PDA1000L apparatus comprises a standard vibrator and terminal-controlling PC software.

The binary granular particles were poured into a cylindrical plexiglass container 10 cm in diameter and 18 cm in height, fixed tightly on the vibrator. The vibrator produces a standard sinusoidal wave $y = A \sin \omega t$, and the detection device on the

*pingwu@sas.ustb.edu.cn

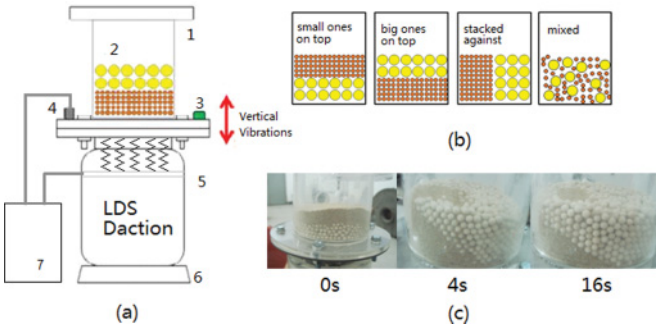

FIG. 1. (Color online) Schematic diagram of the experimental settings. (a) Vibration apparatus. (1) The cylindrical container, (2) the binary granular particles, (3) the horizontal balance detector, (4) the feedback probe, (5) the LDS vibrator, (6) the fixed base on the plane floor, and (7) the controlling systems on the PC. (b) Schematic of the different initial packing states. (c) A typical phase formation process from RBN to BN separation.

container joins a feedback circuit to ensure the accuracy of the vibration parameters.

Three kinds of standard 13X molecular sieve particles were used. Their respective diameters ϕ were 6.00 mm $\pm$ 0.10 mm, 0.75 mm $\pm$ 0.05 mm, and 0.60 mm $\pm$ 0.05 mm, and they have the same actual density $\rho_0 = 1.50$ g/cm^3 $\pm$ 0.05 g/cm^3, i.e., $\rho_l/\rho_s = 1$. Parameters belonging to large and small particles are marked with the subscripts l and s, respectively, such that the total mass ratio $\mu_m = m_l/m_s$, and the diameter ratio $\mu_\varphi = \phi_l/\phi_s$ in expression. The diameter ratio μ_φ can be 10:1 or 8:1 and regular segregation patterns or phases with clearly divided boundaries can be formed in this diameter ratio range. As the small particles are much smaller than large particles in their diameter, the random close packing density of their mixture at rest, ρ_ε, is mainly affected by small particles. In our calculations we took the value constant as $\rho_\varepsilon = 0.75$ g/cm^3 $\pm$ 0.05 g/cm^3.

B. Separation phases

In our experiment, we confirmed that the initial packing state and external disturbance during vibration have no effect on the final separation results. Within the range of the parameters (f from 10 to 90 Hz, Γ from 1.0 to 3.8), a final separation pattern in the container is achieved in 30 s, with a boundary forming between the large and small particles. The patterns include BN, RBN separation, and the transitional forms between them, as shown in Figs. 2(a) and 2(b). Sandwich separation was not observed.

The separation result shown in Figs. 2(a) and 2(b) can be divided into several separation phases. As illustrated in Fig. 2, the light-colored occupation represents the large particles, and the dark-colored region reflects the small particles. Under relatively low (f from 10 to 70 Hz, Γ from 1.0 to 3.8) parameters, a BN phase, a BN transitional (BNT) phase, a RBN transitional (RBNT) phase, and a RBN phase can coexist. These four separation phases remain stable in the experiments.

In a typical BN separation, the large particles cover the small ones, but their segregation forms differ in detail. During vibration, the small particles rise on one side to form a slope, and in some cases, a fountain breaks the top layer of large particles. The term "BN phase" was coined to describe the case in which the slope does not rise to touch the top and connect the fountain circle. After this contact and connection, the BNT phase appears. In phase division, during BN or BNT separation, the mass center of the large particles would always be higher than that of the small ones. Therefore, the division point between BNT and RBNT stands where the respective mass centers of large and small particles bear the same height. The calculation method is discussed in later sections. For the RBN phase, small particles cover the entire top surface, and large particles are brought to the bottom, forming a tilted slope on one side.

When the vibration parameters are relatively high (f from 70 to 90 Hz, Γ from 1.0 to 3.8), oscillating separation patterns are observed, in which the particle system oscillates between the four stable phases, thus appearing unstable. In Refs. [17,18], a similar phenomenon was reported, where the particles act chaotically, and the separation patterns vary with time. We define this situation in the experiment as the oscillating phase.

C. Dynamical equilibrium

In previous studies, complex and versatile convection patterns were reported in granular systems under vertical

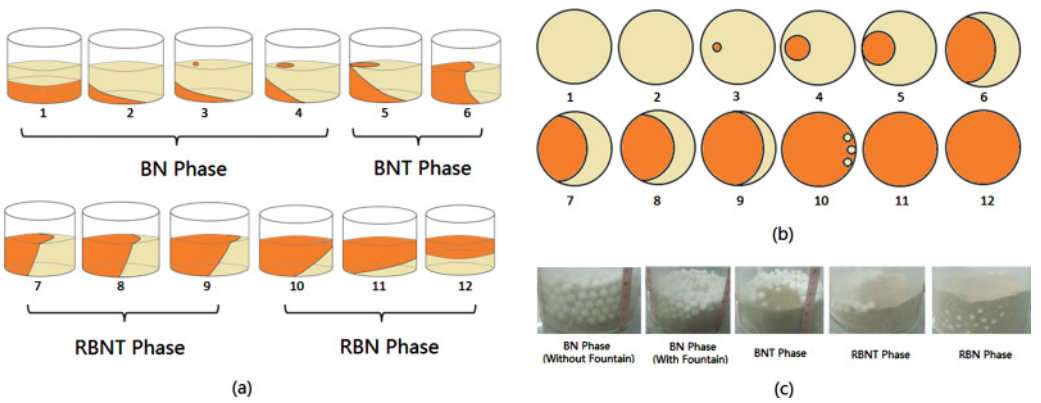

FIG. 2. (Color online) Illustrations of stable separation patterns observed under different vibration parameters. (a) Lateral view, (b) top view, and (c) experimental photos. In these patterns from BN separation to RBN separation, the fountain of small particles grows in size, which is attributed to the phase shift when f decreases from 90 to 10 Hz or when Γ increases from 1.0 to 3.8.

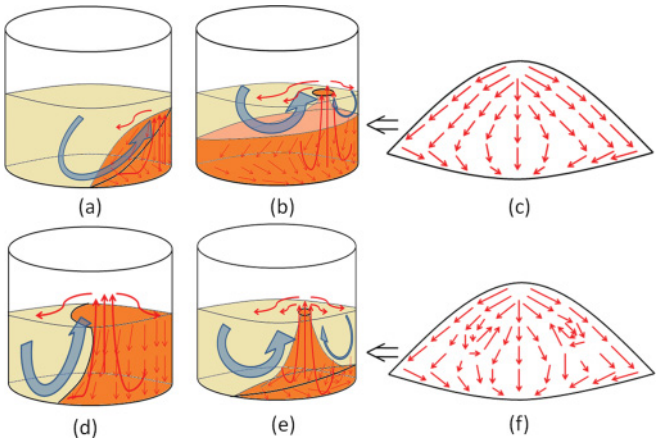

FIG. 3. (Color online) Illustration of the convection modes directly observed from the trajectories of the particles in contact with the cylindrical wall and from the motion of the surface. (a) BN phase without a small particle fountain on the top surface, in which small particles concentrate on one side and circulate. (b) The fountain breaks the top layer, still in the BN phase. (c) Lateral view of convection traces of the small particles in (b). (d) The BNT or RBNT phase, and the fountain's size grows. (e) A typical oscillating phase. Sometimes the fountain vanishes, and a new one emerges elsewhere. (f) Lateral view of the small particles in (e).

vibration [9,17,19,20]. Granular convections in the container [21] and wavy motions [22] were also observed. Usually, when the diameter ratio μ_φ is relatively large, such as 10:1 or 8:1, the small particles tend to fluidize in motion [19,20]. Numerous researchers have attempted to propose complete theories to explain this mechanism [23,24]. We observed different forms of granular convection in the stable phases, as well as different features for the oscillating phase.

In all our experiments, large and small particles each complete a convection cycle. The convection of small particles flows drastically, similar to fountains, with particles rising from the bottom to the top and then scattering off, whereas large particles move slowly. Large and small particles interact with each other by friction and collision to form a dynamical equilibrium in the stable phases.

In the oscillating phase shown in Fig. 3(e), the fountain of smaller particles moves around and the entire structure remains unstable. In Fig. 3(f), we find irregular eddy-shaped traces, indicating that the convection mechanism of the oscillating phase differs from that of the stable phases. Red (thin, light gray) arrows represent the convection trace of the small particles, and blue (thick, dark gray) arrows represent that of the large particles.

III. SCALING METHODS

To study the phases under different vibration and particle system parameters quantitatively, we have defined the phase parameter λ to describe the segregation patterns in these situations. With the total mass of m_l and m_s, the radius of the container's cross section R_0 measured, the packing height of the mixed particles in the container H_p is expressed as

$$H_p = \frac{(m_l + m_s)}{\pi R_0^2 \rho_\varepsilon}. \tag{1}$$

The relation between the large and small particles' respective mass center heights H_l and H_s can be written as

$$\frac{m_s H_s + m_l H_l}{m_s + m_l} = \frac{H_p}{2}. \tag{2}$$

When the large particles completely cover the small ones or when the system forms a complete BN (CBN) separation,

$$H_{l,\mathrm{CBN}} - H_{s,\mathrm{CBN}} = H_p/2. \tag{3}$$

In addition, if the situation is a complete RBN (CRBN) separation,

$$H_{l,\mathrm{CRBN}} - H_{s,\mathrm{CRBN}} = -H_p/2. \tag{4}$$

We propose the phase parameter λ here to be proportional to $H_l - H_s$. If $\lambda > 0$, the system is closer to BN separation, and if $\lambda<0$, it is closer to RBN separation. When $\lambda = 0$, the mass centers of the large and small particles stand at the same height, and this situation becomes a dividing point. $\lambda = -1$ represents a CRBN separation, and $\lambda = 1$ denotes a CBN separation. To describe the transitional states between CRBN and CBN, we define the phase parameter λ as

$$\lambda = \frac{H_l - H_s}{H_p/2}. \tag{5}$$

Combining Eqs. (2) and (5),

$$\lambda = \left(1 + \frac{m_s}{m_l}\right)\left(1 - \frac{2H_s}{H_p}\right). \tag{6}$$

In this equation, the mass center height of the small particles H_s is chosen as the target of the calculation. H_s can be determined via a detailed analysis of the morphological features of the granular system in the Appendixes. We summarize the division of the phases with the phase parameter λ between -1 and 1 in Fig. 4.

IV. EXPERIMENTAL RESULTS

A. f-Γ-λ phase diagram

We selected binary granular particles with the diameter ratio $\mu_\varphi = 10{:}1$ and mass ratios of $\mu_m = 1.0{:}0.5$, $1.0{:}1.0$, $1.0{:}1.5$, and $1.0{:}2.0$. We performed experiments under the initial condition of random packing as shown in Fig. 1(b). An f-Γ-λ phase diagram was scanned with the frequency f from 10 to 90 Hz, 2 Hz stepped, and Γ from 1.0 to 3.8, 0.2 stepped. Each pair of (f,Γ) combinations was set to the device, and after 30 s, stable separation results were obtained. A number of oscillation results took longer to identify. To calculate λ in each condition, we set up geometrical models for each type of separation result (see details in the Appendixes). In each model, the critical geometrical parameters of the separation structure were directly measured. The mass center heights of the large and small particles were calculated thereafter via mathematical analysis.

B. Effect of f and Γ on the separation results

It can be recognized from Fig. 5 that when $\mu_\varphi = 10{:}1$ under the influence of a relatively low f and Γ (f from 10 to 70 Hz, Γ from 1.0 to 3.8), the system exhibits stable separation

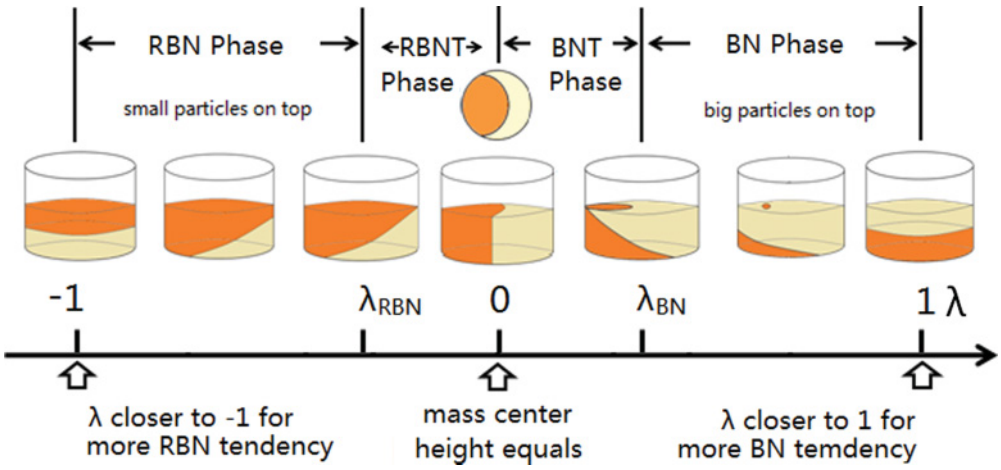

FIG. 4. (Color online) Phase parameter λ within [−1,1] and the range for each phase. When the fountain of the small particles grows and touches the wall, the phase is changed from BN to BNT, and λ is marked as λ_{BN} at this critical point. λ = 0 states the dividing point between BNT and RBNT. When small particles cover the entire top surface and RBNT transforms to RBN, λ is marked as λ_{RBN}. The following phase diagrams should be related to this criterion to obtain the separation result according to the value of λ.

states. When f alone is increased and Γ is kept constant, the tendency of the particle system toward the BN phase increases. In contrast, when Γ alone is increased and f is kept constant, the tendency toward the RBN phase increases. In terms of the stable phases, these tendencies are manifested.

For the oscillating phase, two diagrams were scanned with μ_m = 1.0:1.0 in the same condition as that in Figs. 5(2) and 6. The separation results were observed to be moving in the regions of the oscillating phase, with shifting peaks and valleys that can be recorded through measurements of the geometrical structure and a calculation of the phase parameter λ.

C. Effect of μ_m and μ_φ on the separation results

As can be summarized from Figs. 5(1)–5(4), with an increasing mass proportion of the small particles, the system's tendency toward the RBN phase grows. When μ_m = 1.0:0.5, only the BNT and BN phases are present in the stable region. When μ_m = 1.0:1.0, the RBNT phase appears in the low f and the high Γ region and enlarges when μ_m = 1.0:1.5, pushing the other phases to the right of the diagram. When μ_m = 1.0:2.0, the RBN, RBNT, and BNT phases are present within the range of parameters of the device.

A similar experiment was performed with μ_φ = 8:1 and μ_m = 1.0:1.0, as illustrated in Fig. 7. Compared with the diagram when μ_m = 10:1, the tendency toward the BN phase is stronger in μ_φ = 8:1, and the area of the oscillating phase expands.

V. DISCUSSIONS

In previous studies, the separation results under different parameter settings were mostly definite BN or RBN [11–17, 25]. However, we observed the transitional separation states between these two when μ_φ = 10:1 or 8:1, as mentioned above. The monodirectional effects in stable separation phases can be summarized as follows: The system's tendency toward BN separation increases with f and μ_m, and decreases with Γ and μ_φ. The effects of f and Γ here come in accordance with the conclusion drawn from the dividing line between definite BN and RBN in Ref. [11], where 10 mm polyurethane and 4 mm glass spheres were applied in their experiments, with μ_φ low as 2.5.

To establish a judging criterion, the method of comparing granular temperatures was proposed in Ref. [15]. In this method, if μ_φ is smaller than the inverse of ρ_l/ρ_s, the particle mixture should show a Brazilian nut effect, and vice versa [11]. The influence of Γ is added to the criterion as in Ref. [25], with a modifying factor of $\alpha(\Gamma)$ acquired through experimental data, and μ_φ takes the value from 0 to 3. In Ref. [25], it is proposed that, if μ_φ is smaller than $1+\alpha(\Gamma)(\rho_l/\rho_s-1)$, the particle system would finally exhibit a BN separation, and vice versa [25]. Accordingly, the final separation result for such a system with μ_φ = 10:1 or 8:1 should have been definitely reversed Brazilian nut separation when ρ_l/ρ_s = 1. However, in our experiments the separation states between BN and RBN at these system settings are transitional, rather than being definite. What used to be a "mixed" state, or the dividing dots of definite BN and RBN results that only exist in a very narrow scope as described in Refs. [11,25], has stretched to the entire phase diagram.

Of all the separation results, a CRBN (λ =−1) is actually never achieved. Only a very strong tendency for RBN is observed when μ_m is quite low [e.g., 1.0:1.5 or 1.0:2.0 in Figs. 5(3) and 5(4)], with relatively low f and high Γ. Actually, when μ_φ is high as this set, i.e., 10:1 or 8:1, the small particles become fluidized in their motional behavior [19,20]. The mechanism of percolation [4,5] would play an important role, when the small particles rise and tend to cover the large ones. This makes a CRBN impossible and the separation result appear BN intended all the time, or λ > 0 in most cases. The diameter ratio in Ref. [25] is 3 to the upmost, and we indicate that for higher values, new approaches considering the influence of percolation, and proper methods describing the transitional states between definite BN and RBN should be included in the expression of granular temperatures.

Abnormal points in the stable phase region were also observed in the phase diagrams. For example, in Fig. 5(2), when f = 20–30 Hz, Γ = 1.5–2.0, the BN phase is observed within the region of the BNT phase. In Fig. 5(3), when f =

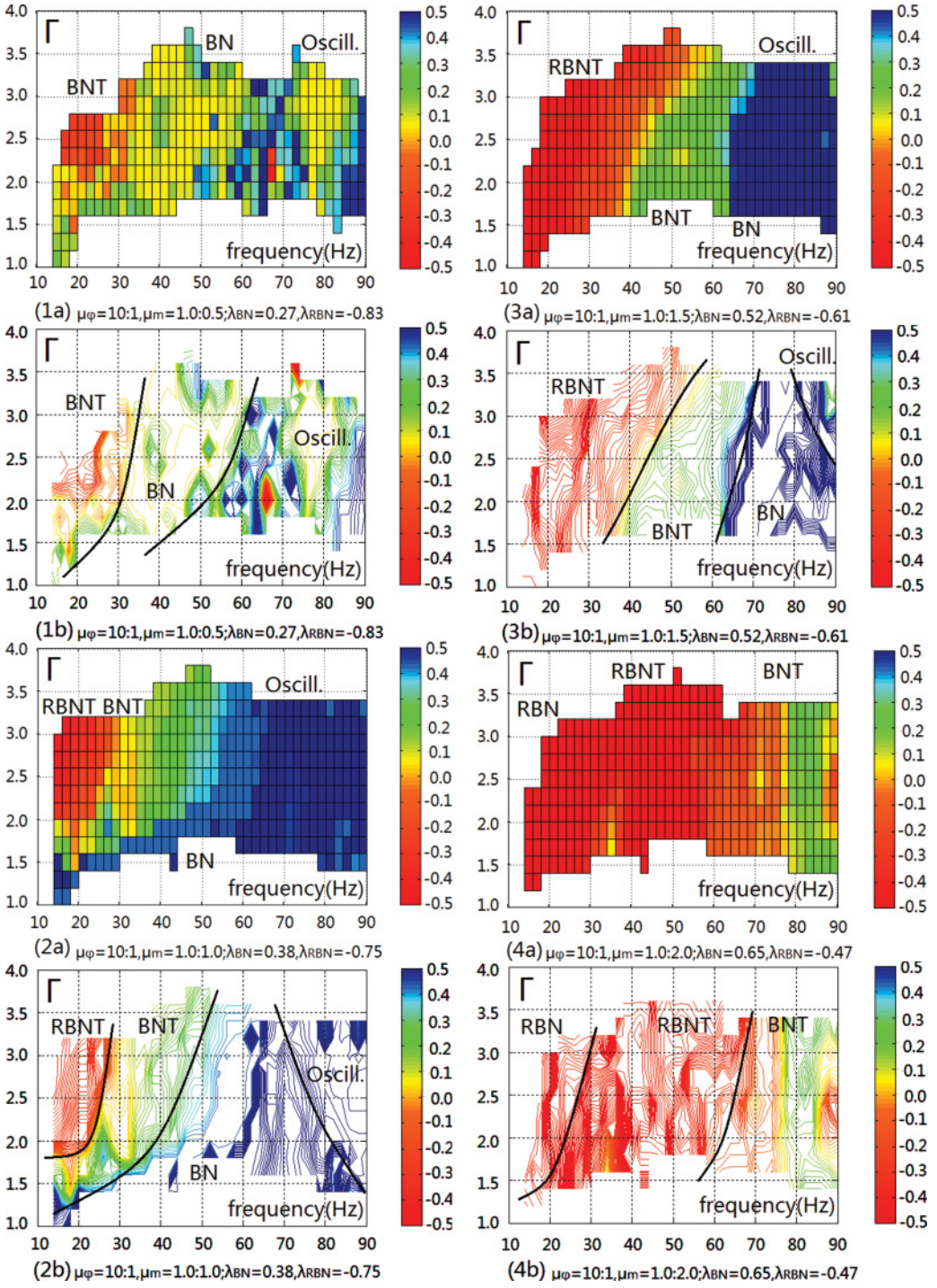

FIG. 5. (Color online) f-Γ-λ phase diagrams and their respective contour maps with the binary granular particles' diameter ratio $\mu_\varphi =$ 10:1 and mass ratios $\mu_m =$ 1.0:0.5, 1.0:1.0, 1.0:1.5, and 1.0:2.0. The value of λ on the z axis is marked with the color (grayscale) bar, and the four phase diagrams include phases of RBN, RBNT, BNT, and BN with the dividing value of the phase parameter λ marked aside. Boundaries between the stable phase and the oscillating phase were acquired through repeated experiments. The situation when λ takes the value beyond ±0.5 is quite rare, therefore we maintain the color of blue (dark gray) or red (light gray) for λ within $[-1, -0.5]$ and [0.5,1], respectively, for better presentation and for easier comparison.

50–60Hz, $\Gamma = 2.0$–2.5, the RBNT phase is observed within the region of the BNT phase. Moreover, in the phase diagrams, the separation result with a relatively high f,Γ are unstable and oscillating beyond some f and Γ parameters marked in each phase diagram as the oscillating phase.

We propose a method based on energy conservation relations to explain the behavior of the binary particle mixtures at this diameter ratio qualitatively. As discussed above, the four parameters, namely, frequency f, dimensionless acceleration Γ, total mass ratio μ_m, and diameter ratio μ_φ, significantly

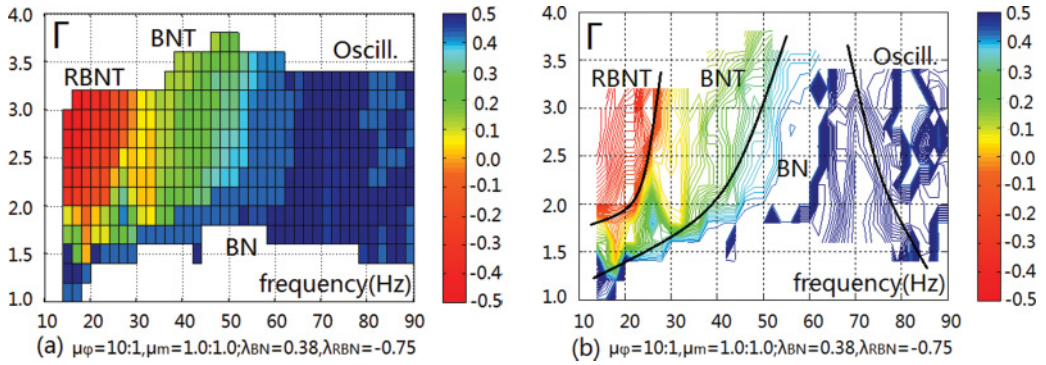

FIG. 6. (Color online) Comparison [with Fig. 5(2)] between the stable phases and the oscillating phase with relatively high f and Γ parameters. Only the region of the oscillating phase changed significantly in this comparison.

affect the separation pattern of the binary granular system. We attempted to explain the experimental result of the stable phases by analyzing the distribution of dissipated energy during vibration. The frequency exerted on the granular system is several tens of Hz, and a particle's motion in the system involves pressing and frictional forces. Therefore, some relaxation time from the external excitations is reasonable. The average incoming power P can be expressed as

$$P = \frac{1}{T}\int_0^T \frac{1}{2}(m_l + m_s)(-A\omega \sin \omega t)^2 dt$$
$$= \frac{(m_l + m_s)A^2\omega^2}{4} = \frac{(m_l + m_s)g^2}{16\pi^2}\frac{\Gamma^2}{f^2}. \quad (7)$$

Apparently, P is proportional to the square of Γ and inversely proportional to the square of f. In our experiment, the convection of the small particles is much faster than that of the large ones, and a distribution of the external energy input occurs in the respective convections of the large and small particles. Feitosa [26] proposed that energy primarily dissipates through the bouncing and friction in convection cycles, and Hou [27] confirmed that small particles have more dissipated energy during convection.

As presented in (7), when other parameters remain constant and only f increases, P decreases, and the energy supporting the granular convection and dissipation also decreases. Thus, small particles tend to move slower and segregate down into the bottom layer. When Γ increases, P also increases, and small particles gain more energy support for convection, easily breaking the top surface to form a fountain. Hence, the system's tendency toward the RBN phase is enhanced. The smaller the particles are, the more fluidized they become, consequently sharing more dissipated energy. A stronger tendency toward the RBN phase is thus observed. In addition, when μ_m increases, the small particles share a decreasing amount of dissipating energy. Hence, their convection slows down, and the system's tendency toward the BN phase increases. The distribution of dissipating energy and the convection pattern of small particles played an important role in this experiment.

As for the physical mechanism of the oscillating phase, an unified explanation is needed. A number of researchers believe that the boundary conditions significantly affect the oscillating system [18,28] and that the behavior of particle layers is strongly influenced by f in this region [29]. Chaos can be found with relatively strong vibrations [30], and more complex patterns may be observed under other parameters [31]. The mechanism of the abnormal points in the stable phase region and the oscillating phase must be more carefully investigated via theories, simulations, and experiments.

VI. CONCLUSIONS

In conclusion, we performed laboratory tests on the binary granular particle system with diameter ratios of 10:1 and 8:1,

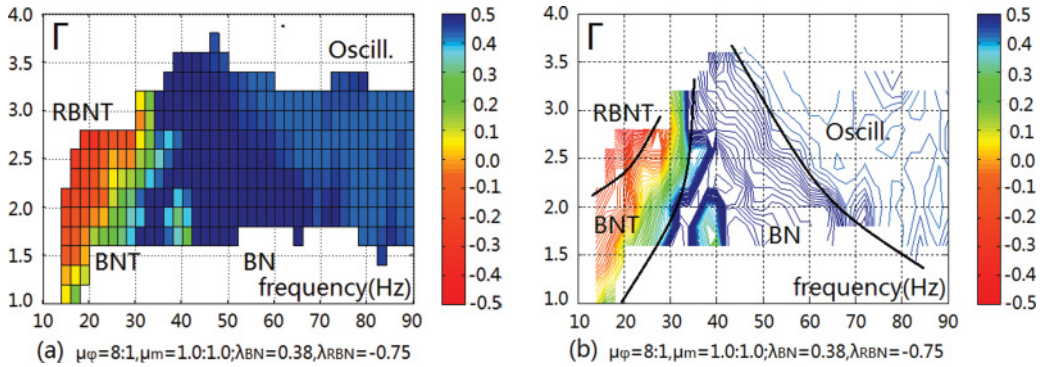

FIG. 7. (Color online) Comparison [with Fig. 5(2)] of the phase diagrams when μ_φ = 8:1 and 10:1, with all other parameters being the same. The general rules mentioned above in the stable phase region are maintained, and the abnormal points can be found when μ_φ = 8:1, f = 30–40 Hz, and Γ = 1.5–2.0.

in which a continuous array of changing patterns between BN and RBN separation are observed, sketched, and compared in elaborate details. The experimental results of these continually changing patterns revealed the unique characteristics of the granular system under these specific parameters. The separation patterns generally remain stable when f and Γ are relatively low, and the stable phases BN, BNT, RBNT, and RBN can be divided according to their geometrical features. An oscillating result emerges when f and Γ are relatively high, and the system forms an oscillating phase. A phase parameter λ that concerns the difference in the respective mass center heights of the large and small particles is defined between -1 and 1 to characterize the system's tendency toward CRBN or CBN. f-Γ-λ phase diagrams clearly described the ranges of these separation phases, and the comparisons among the diagrams offered explicit insight into the effect of each of the vibration and system parameters. In stable phases, the system's tendency toward BN separation increases with f and μ_m, and decreases with Γ and μ_φ. These phenomena can be preliminarily explained via an analysis of the dissipating energy during vibration, with more to be discovered on the constantly transforming patterns of the oscillating phase.

ACKNOWLEDGMENTS

This work was supported by the National Natural Science Foundation of China, Grant No. 51076010.

APPENDIX A: CALCULATION METHODS FOR THE BN PHASE WITH A FOUNTAIN

We observed the separation surfaces via experimentation. The surface between the two kinds of particles presents conical or flat planes after dynamical equilibrium is achieved. Therefore, we have set up mathematical models accordingly to get H_s.

The pattern with a fountain of small particles in the BN phase is the most common separation result in our experiments. When the small particles do not thoroughly cover the bottom layer, the geometrical structure of the separation result is presented in Fig. 8. The directly measured value is H_d. The values calculated thereafter are R_s, R_c, and R_b.

As illustrated in Fig. 8, we focus on the structure of the small particles. To calculate the mass center of the small particles, we adopt the polar coordinate system and fix the origin point on M_0. The lateral shape of the fountain structure inside the large particles was found to be a conical surface via experimentation. After careful measurements, we found that in all cases where the small particles break the top layer to form a fountain, the tilting angle of the conical surface φ_d remains constant at approximately 40°. This condition occurs when the small particles upsurge and push the big particles around, through which a balance is achieved. This balance is delicately kept during the dynamical equilibrium process of the binary interactive convections. Therefore, we derive

$$\varphi_d = 40^\circ. \tag{A1}$$

Other relations of the parameters describing the structure can be written according to Fig. 8:

$$\tan\varphi_d = \frac{H_p - H_d}{R_c - R_s}, \tag{A2}$$

$$\tan\varphi_d = \frac{H_p}{R_b - R_c - R_s}. \tag{A3}$$

We selected the height of the slope H_d, which can be measured and recorded with ease, as the critical parameter in this structure. Apparently, if the container's shape and the total mass of large and small particles are determined, three unknowns remain, namely, R_s, R_c, and R_b. The equations to solve these unknowns are the mass conservation rule combined with (A2) and (A3).

For easy integration, we cut the structure of small particles into three parts. The first part, V_1, is the wrapping shape of the central column with radius R_s and height H_p. This part is cut left to the planes M_1FM_0 and M_1EM_0. In this ρ-θ-z polar coordinate system centered in M_0, the outer rim of the container at the bottom, that is, a circle with radius R_0, should be written as

$$\rho_2(\theta) = \cos\theta(R_0 - R_c) + \sqrt{\cos^2\theta(R_0 - R_c)^2 + \left(2R_0R_c - R_c^2\right)}. \tag{A4}$$

According to the geometrical structure, the conical surface can be expressed as

$$z_1(\rho) = -\tan\varphi_d\rho + (R_c\tan\varphi_d + H_d). \tag{A5}$$

In addition, in ΔM_0EO_0, the following formula presents in view of the law of cosines in triangles:

$$\theta_s = \arccos\frac{(R_0 - R_c)^2 + (R_b - R_c)^2 - R_0^2}{2(R_0 - R_c)(R_b - R_c)}. \tag{A6}$$

The volume of the first part is

$$\begin{aligned} V_1 &= \int_{\theta_s}^{2\pi-\theta_s}\int_{R_s}^{\rho_2(\theta)}\int_0^{z_1(\rho)}\rho dz d\rho d\theta \\ &= \int_{\theta_s}^{2\pi-\theta_s} -\frac{1}{3}\tan\varphi_d\left[\rho_2^3(\theta) - R_s^3\right] \\ &\quad + \frac{1}{2}(R_c\tan\varphi_d + H_d)\left[\rho_2^2(\theta) - R_s^2\right]d\theta. \end{aligned} \tag{A7}$$

The mass center height of this part is

$$\begin{aligned} H_{s1} &= \frac{1}{V_1}\int_{\theta_s}^{2\pi-\theta_s}\int_{R_s}^{\rho_2(\theta)}\int_0^{z_1(\rho)} z\rho dz d\rho d\theta \\ &= \frac{1}{V_1}\int_{\theta_s}^{2\pi-\theta_s}\frac{1}{8}\tan^2\varphi_d\left[\rho_2^4(\theta) - R_s^4\right] \\ &\quad - \frac{1}{3}\tan\varphi_d(R_c\tan\varphi_d + H_d)\left[\rho_2^3(\theta) - R_s^3\right] \\ &\quad + \frac{1}{4}(R_c\tan\varphi_d + H_d)^2\left[\rho_2^2(\theta) - R_s^2\right]d\theta. \end{aligned} \tag{A8}$$

For the second part, the central column is

$$V_2 = \pi R_s^2 H_p, \tag{A9}$$

$$H_{s2} = \frac{H_p}{2}. \tag{A10}$$

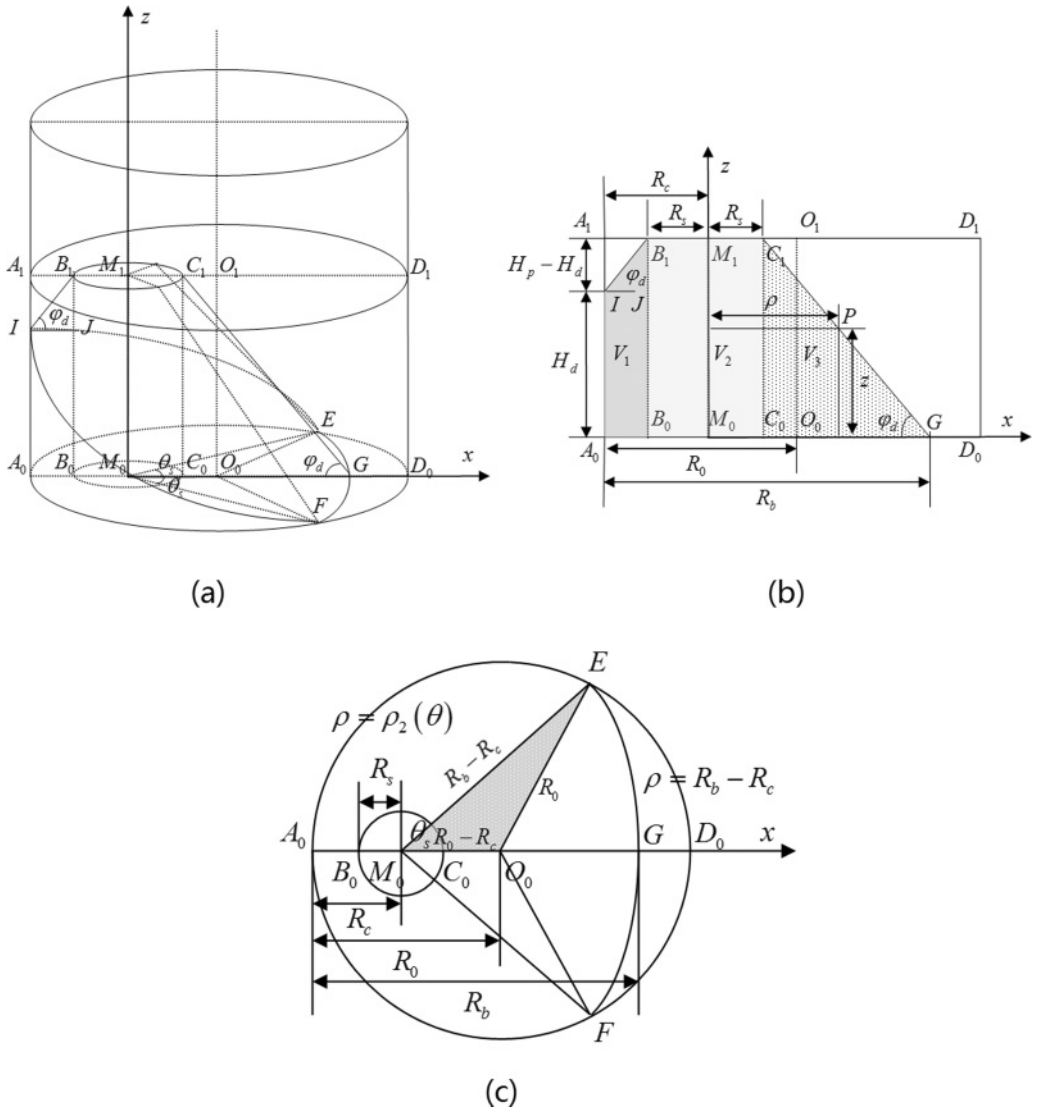

FIG. 8. Schematic diagram of the BN phase with a small particle fountain, when small particles do not cover the entire bottom. The polar coordinate system takes M_0 as the origin point, perpendicularly beneath the fountain center M_1 on the top surface. Critical parameters in this structure, such as R_0, R_c, R_b, and H_d, are also marked. In this coordinate system, Arc EF and EA_0F are each written in their polar forms.

In addition, for the rest of the structure or the third part,

$$V_3 = \int_{-\theta_s}^{\theta_s}\int_{R_s}^{R_b-R_c}\int_0^{z_1(\rho)} \rho dz d\rho d\theta$$
$$= 2\theta_s\left\{-\frac{1}{3}\tan\varphi_d\left[(R_b-R_c)^3 - R_s^3\right]\right.$$
$$\left. + \frac{1}{2}(R_c\tan\varphi_d + H_d)\left[(R_b-R_c)^2 - R_s^2\right]\right\}, \quad \text{(A11)}$$

$$H_{s3} = \frac{1}{V_3}\int_{-\theta_s}^{\theta_s}\int_{R_s}^{R_b-R_c}\int_0^{z_1(\rho)} z\rho dz d\rho d\theta$$
$$= \frac{1}{V_3}2\theta_s\left\{\frac{1}{8}\tan^2\varphi_d\left[(R_b-R_c)^4 - R_s^4\right]\right.$$
$$- \frac{1}{3}\tan\varphi_d(R_c\tan\varphi_d + H_d)\left[(R_b-R_c)^3 - R_s^3\right]$$
$$\left. + \frac{1}{4}(R_c\tan\varphi_d + H_d)^2\left[(R_b-R_c)^2 - R_s^2\right]\right\}. \quad \text{(A12)}$$

The three parts together comprise the entire volume of the small particles,

$$V_1 + V_2 + V_3 = V_s = m_s/\rho_\varepsilon. \quad \text{(A13)}$$

By combining Eqs. (A2), (A3), and (A13), the three unknowns, namely, R_s, R_c, and R_b, can be solved via numerical methods. We applied MATLAB2010A programs in our work, and the experimental results were perfectly obtained via this calculation method.

With these unknowns solved, we calculated H_s through (A7)–(A12):

$$H_s = \frac{V_1H_{s1} + V_2H_{s2} + V_3H_{s3}}{V_s}. \quad \text{(A14)}$$

Furthermore, we were able to determine the phase parameter λ in Eq. (6).

When the small particles thoroughly cover the bottom layer and heap to the height of H_b on the other side, the geometrical structure of the separation result is presented in Fig. 9. The

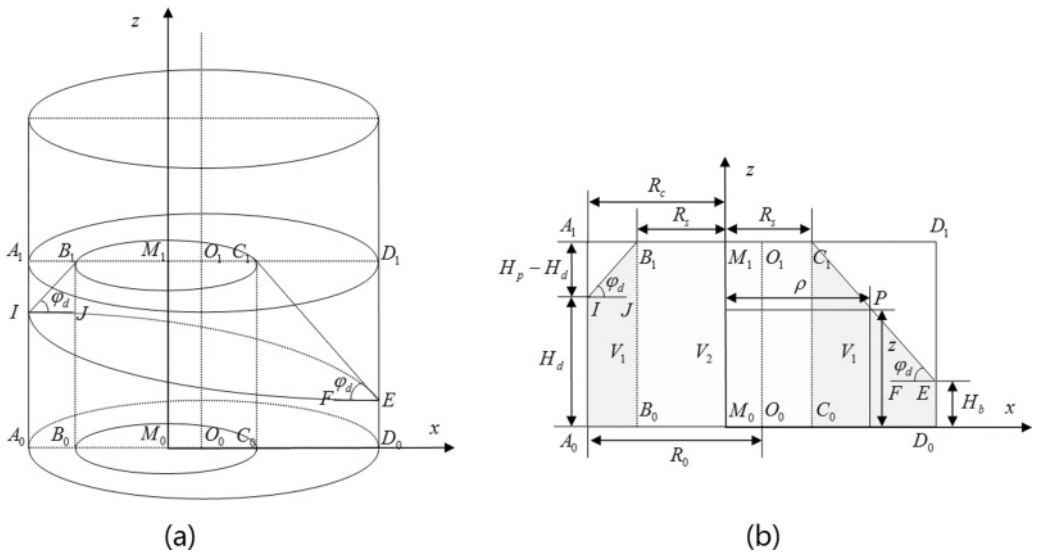

FIG. 9. Schematic diagram of the BN phase with a small particle fountain, wherein small particles cover the entire bottom layer and heap on the other side to a height of H_b.

directly measured value is H_d. The values calculated thereafter are R_s, R_c, and H_b.

The structure of small particles is cut into two parts in the calculation. The outer ring occupies V_1 and the central column V_2. The mathematical form of the conical surface remains as in (A5), and the geometrical features can be written as

$$\tan\varphi_d = \frac{H_p - H_d}{R_c - R_s}, \tag{A15}$$

$$\tan\varphi_d = \frac{H_p - H_b}{2R_0 - R_c - R_s}. \tag{A16}$$

For the first part,

$$\begin{aligned} V_1 &= \int_0^{2\pi}\int_{R_s}^{\rho_2(\theta)}\int_0^{z_1(\rho)} \rho dz d\rho d\theta \\ &= \int_0^{2\pi} -\frac{1}{3}\tan\varphi_d\left[\rho_2^3(\theta) - R_s^3\right] \\ &\quad + \frac{1}{2}(R_c\tan\varphi_d + H_d)\left[\rho_2^2(\theta) - R_s^2\right]d\theta, \end{aligned} \tag{A17}$$

$$\begin{aligned} H_{s1} &= \frac{1}{V_1}\int_0^{2\pi}\int_{R_s}^{\rho_2(\theta)}\int_0^{z_1(\rho)} z\rho dz d\rho d\theta \\ &= \frac{1}{V_1}\int_0^{2\pi} \frac{1}{8}\tan^2\varphi_d\left[\rho_2^4(\theta) - R_s^4\right] \\ &\quad - \frac{1}{3}\tan\varphi_d(R_c\tan\varphi_d + H_d)\left[\rho_2^3(\theta) - R_s^3\right] \\ &\quad + \frac{1}{4}(R_c\tan\varphi_d + H_d)^2\left[\rho_2^2(\theta) - R_s^2\right]d\theta. \end{aligned} \tag{A18}$$

For the second part,

$$V_2 = \pi R_s^2 H_p, \tag{A19}$$

$$H_{s2} = \frac{H_p}{2}. \tag{A20}$$

The two parts together make up the whole volume of the small particles,

$$V_1 + V_2 = V_s = m_s/\rho_\varepsilon. \tag{A21}$$

Equations (A15), (A16), and (A21) were solved with numerical methods, and we can determine the unknowns, namely, H_b, R_c and R_s. With (A17)–(A21), we can determine H_s:

$$H_s = \frac{V_1 H_{s1} + V_2 H_{s2}}{V_s}. \tag{A22}$$

Therefore, through Eq. (6), the phase parameter λ is determined.

APPENDIX B: CALCULATION METHODS FOR THE BN PHASE WITHOUT A FOUNTAIN

For the cases in which the large particles cover the top layer and the fountain is suppressed below, the interface should theoretically be a conical surface, as in Figs. 10 and 11, where small particles either cover the bottom or do not. For the BN phase with a fountain, φ_d is considered to have a fixed value of 40°. We removed the layers of large and small particles from top to bottom and discovered that, in cases where the fountain is suppressed by the upper large particles, the angle φ decreases, eventually reaching 0 when CBN separation is achieved. In CBN separation, the small particles are still in convection when the fountain becomes flat, with a minimum height being

$$H_{\min} = \frac{m_s}{\pi R_0^2 \rho_\varepsilon}. \tag{B1}$$

We introduce a linear assumption for tan φ here, when the highest point of the suppressed fountain gains a height

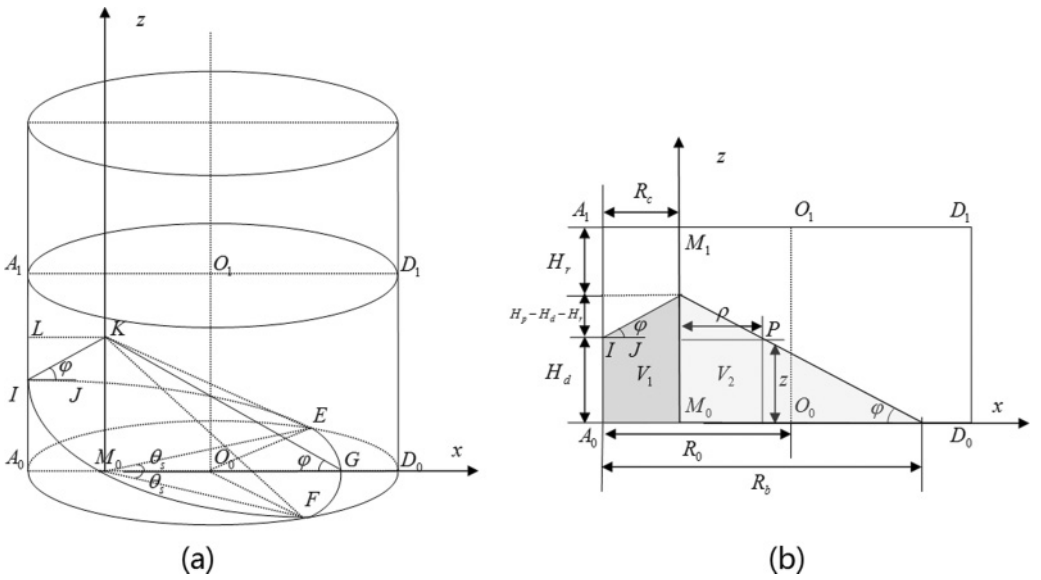

FIG. 10. Schematic diagram of the BN Phase without a small particle fountain, where the small particles do not cover the entire bottom. The structure of the small particles is cut into two parts. The geometrical pattern on the bottom is similar to that in FIG. 8 (c), only by canceling the R_s circle cast from above.

of $H_p - H_r$:

$$\tan\varphi = \tan\varphi_d \frac{H_p - H_r - H_{\min}}{H_p - H_{\min}}. \tag{B2}$$

The directly measured value is H_d. The values calculated thereafter are R_s, R_c, and H_r.

Geometrically, we derive

$$\tan\varphi = \frac{H_p - H_d - H_r}{R_c}, \tag{B3}$$

$$\tan\varphi = \frac{H_p - H_r}{R_b - R_c}. \tag{B4}$$

The conical surface can be expressed as

$$z_2(\rho) = -\tan\varphi\,\rho + (H_p - H_r). \tag{B5}$$

For the first part,

$$V_1 = \int_{-\theta_s}^{\theta_s}\int_0^{R_b-R_c}\int_0^{z_2(\rho)} \rho dz d\rho d\theta = 2\theta_s\left[-\frac{1}{3}\tan\varphi(R_b - R_c)^3 + \frac{1}{2}(H_p - H_r)(R_b - R_c)^2\right], \tag{B6}$$

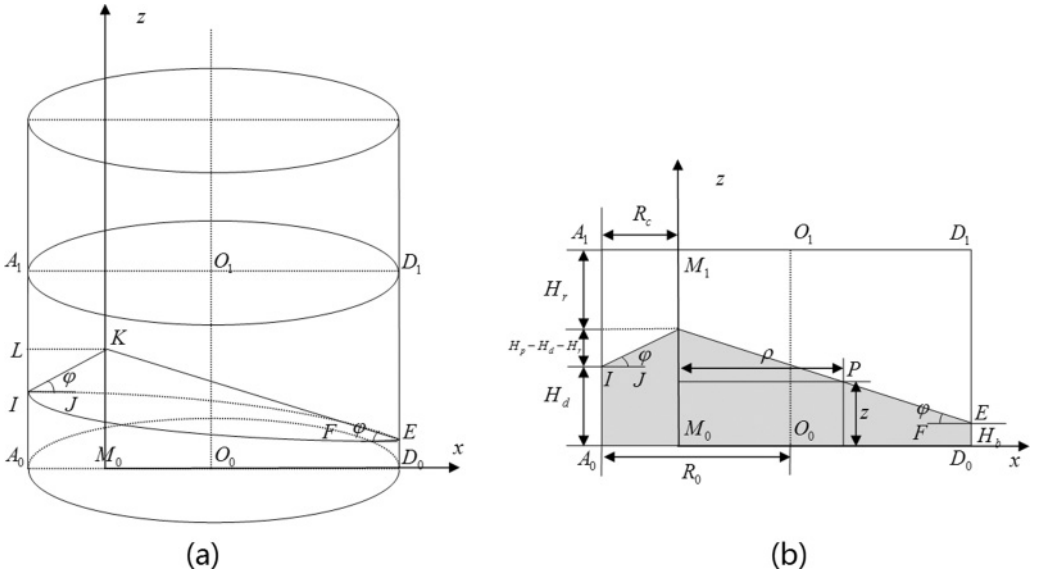

FIG. 11. Schematic diagram of the BN phase without a small particle fountain, where small particles cover the entire bottom. The structure of the small particles is considered as a whole in integration calculations.

$$H_{s1} = \frac{1}{V_1}\int_{-\theta_s}^{\theta_s}\int_0^{R_b-R_c}\int_0^{z_2(\rho)} z\rho dz d\rho d\theta$$
$$= \frac{1}{V_1} 2\theta_s \left[\frac{1}{8}\tan^2\varphi (R_b - R_c)^4 - \frac{1}{3}\tan\varphi (H_p - H_r) \times (R_b - R_c)^3 + \frac{1}{4}(H_p - H_r)^2 (R_b - R_c)^2\right]. \quad \text{(B7)}$$

For the second part,

$$V_2 = \int_{\theta_s}^{2\pi-\theta_s}\int_0^{\rho_2(\theta)}\int_0^{z_2(\rho)} \rho dz d\rho d\theta$$
$$= \int_{\theta_s}^{2\pi-\theta_s} -\frac{1}{3}\tan\varphi\, \rho_2^3(\theta) + \frac{1}{2}(H_p - H_r)\rho_2^2(\theta) d\theta, \quad \text{(B8)}$$

$$H_{s2} = \frac{1}{V_2}\int_{\theta_s}^{2\pi-\theta_s}\int_0^{\rho_2(\theta)}\int_0^{z_2(\rho)} z\rho dz d\rho d\theta$$
$$= \frac{1}{V_2}\int_{\theta_s}^{2\pi-\theta_s} \frac{1}{8}\tan^3\varphi\, \rho_2^4(\theta) - \frac{1}{3}\tan\varphi (H_p - H_r)\rho_2^3(\theta) + \frac{1}{4}(H_p - H_r)^2\rho_2^2(\theta) d\theta. \quad \text{(B9)}$$

As above, with a measured H_d and Eqs. (B3), (B4), and (A21), all the other parameters, namely, R_c, R_b, and H_r, are determined. Subsequently, through (B6)–(B9) and (A22), H_s is calculated, in addition to λ in (6).

In another situation, small particles cover the bottom, as shown in Fig. 11. The directly measured value is H_d. The values calculated thereafter are R_c, H_b, and H_r.

Geometrically, we derive

$$\tan\varphi = \frac{H_p - H_d - H_r}{R_c}, \quad \text{(B10)}$$

$$\tan\varphi = \frac{H_p - H_r - H_b}{2R_0 - R_c}. \quad \text{(B11)}$$

The conical surface can be expressed as in (B5), and for the whole structure,

$$V_s = \int_0^{2\pi}\int_0^{\rho_2(\theta)}\int_0^{z_2(\rho)} \rho dz d\rho d\theta$$
$$= \int_0^{2\pi} -\frac{1}{3}\tan\varphi\, \rho_2^3(\theta) + \frac{1}{2}(H_p - H_r)\rho_2^2(\theta) d\theta, \quad \text{(B12)}$$

$$H_s = \frac{1}{V_s}\int_0^{2\pi}\int_0^{\rho_2(\theta)}\int_0^{z_2(\rho)} z\rho dz d\rho d\theta$$
$$= \frac{1}{V_s}\int_0^{2\pi} \frac{1}{8}\tan^3\varphi\, \rho_2^4(\theta) - \frac{1}{3}\tan\varphi (H_p - H_r)\rho_2^3(\theta) + \frac{1}{4}(H_p - H_r)^2\rho_2^2(\theta) d\theta. \quad \text{(B13)}$$

Therefore, through Eq. (6), the phase parameter λ is determined.

APPENDIX C: CALCULATION METHODS FOR THE BNT AND RBNT PHASES

In the BNT and RBNT phases, the fountain of the small particles grows and connects with the slope on one side. This interaction face remains a conical surface, as illustrated in Fig. 12 for the BNT phase and Fig. 13 for the RBNT phase. The directly measured values are R_c and R_{st}. The value calculated thereafter is R_{sb}.

In $\Delta M_0 I_0 O_0$, in view of the law of cosines in triangles, we obtain

$$\theta_{st} = \arccos\frac{(R_0 - R_c)^2 + R_{st}^2 - R_0^2}{2R_{st}(R_0 - R_c)}. \quad \text{(C1)}$$

In $\Delta M_0 E_0 O_0$, we derive

$$\theta_{sb} = \arccos\frac{(R_0 - R_c)^2 + R_{sb}^2 - R_0^2}{2R_{sb}(R_0 - R_c)}. \quad \text{(C2)}$$

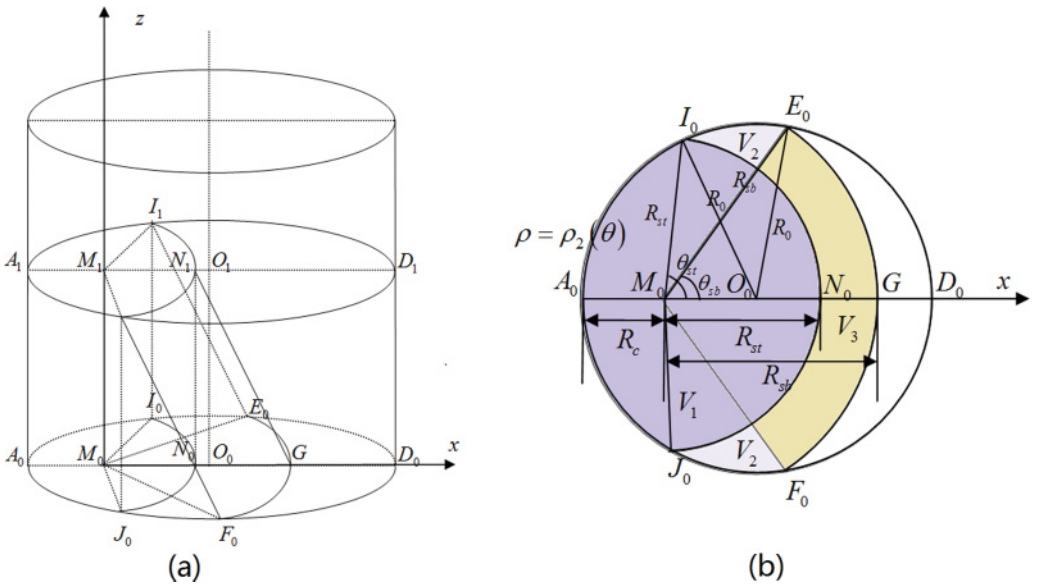

FIG. 12. (Color online) Schematic diagram for the BNT phase. The small particles are divided into three parts. In the same polar coordinate system, the outer rim circle in (b) is still expressed as $\rho_2(\theta)$ in Eq. (A4).

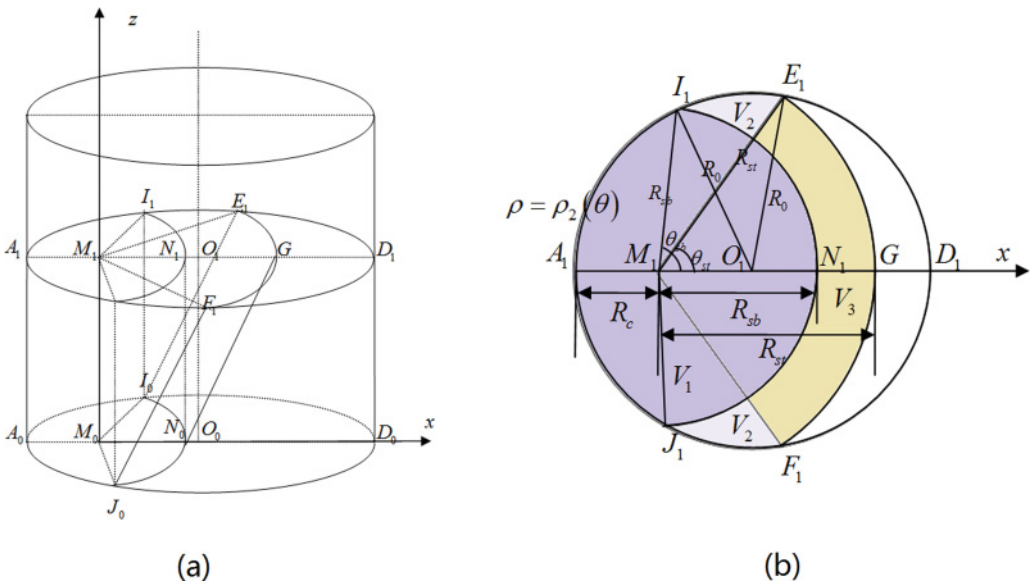

FIG. 13. (Color online) Schematic diagram for the RBNT phase. The structure of small particles is also divided into three parts, and the mathematical form of $\rho_2(\theta)$ is the same as that in Fig. 12.

The conical form of the interface is therefore

$$z_3(\rho) = \frac{H_p}{R_{st} - R_{sb}}(\rho - R_{sb}). \tag{C3}$$

For the first part,

$$V_1 = \left(\pi R_{st}^2 \frac{2\theta_{st}}{2\pi} + \int_{\theta_{st}}^{2\pi-\theta_{st}} \int_0^{\rho_2(\theta)} \rho d\rho d\theta\right) H_p$$
$$= \left(R_{st}^2 \theta_{st} + \frac{1}{2}\int_{\theta_{st}}^{2\pi-\theta_{st}} \rho_2^2(\theta) d\theta\right) H_p, \tag{C4}$$
$$H_{s1} = H_p/2. \tag{C5}$$

For the second part,

$$V_2 = 2\int_{\theta_{sb}}^{\theta_{st}} \int_{R_{st}}^{\rho_2(\theta)} \int_0^{z_3(\rho)} \rho dz d\rho d\theta$$
$$= \frac{2H_p}{R_{st} - R_{sb}} \int_{\theta_{sb}}^{\theta_{st}} \frac{1}{3}\left[\rho_2^3(\theta) - R_{st}^3\right]$$
$$- \frac{1}{2} R_{sb}\left[\rho_2^2(\theta) - R_{st}^2\right] d\theta, \tag{C6}$$

$$H_{s2} = \frac{1}{V_2/2}\int_{\theta_{sb}}^{\theta_{st}} \int_{R_{st}}^{\rho_2(\theta)} \int_0^{z_3(\rho)} \rho z dz d\rho d\theta$$
$$= \frac{1}{V_2}\left(\frac{H_p}{R_{st} - R_{sb}}\right)^2 \int_{\theta_{sb}}^{\theta_{st}} \frac{1}{4}\left[\rho_2^4(\theta) - R_{st}^4\right]$$
$$- \frac{2}{3} R_{sb}\left[\rho_2^3(\theta) - R_{st}^3\right] + \frac{1}{2} R_{sb}^2\left[\rho_2^2(\theta) - R_{st}^2\right] d\theta. \tag{C7}$$

For the third part,

$$V_3 = \int_{-\theta_{sb}}^{\theta_{sb}} \int_{R_{st}}^{R_{sb}} \int_0^{z_3(\rho)} \rho dz d\rho d\theta$$
$$= \frac{1}{3} H_p \theta_{sb}(R_{sb} - R_{st})(2R_{sb} + R_{st}), \tag{C8}$$

$$H_{s3} = \frac{1}{V_3}\int_{-\theta_{sb}}^{\theta_{sb}} \int_{R_{st}}^{R_{sb}} \int_0^{z_3(\rho)} \rho z dz d\rho d\theta$$
$$= \frac{1}{6V_3} H_p^2 \theta_{sb}(R_{sb} - R_{st})(R_{sb} + 3R_{st}). \tag{C9}$$

Through Eqs. (C4), (C6), (C8), and (A13), R_{sb} is determined. H_s is calculated through (A14), in addition to λ in (6). The directly measured values are R_c and R_{st}. The value calculated thereafter is R_{sb}.

In $\Delta M_1 I_1 O_1$, we obtain

$$\theta_{sb} = \arccos \frac{(R_0 - R_c)^2 + R_{sb}^2 - R_0^2}{2R_{sb}(R_0 - R_c)}. \tag{C10}$$

In addition, in $\Delta M_1 E_1 O_1$, we derive

$$\theta_{st} = \arccos \frac{(R_0 - R_c)^2 + R_{st}^2 - R_0^2}{2R_{st}(R_0 - R_c)}. \tag{C11}$$

The conical form of the interface is consistent with (C3), and for the first part,

$$V_1 = \left(\pi R_{sb}^2 \frac{2\theta_{sb}}{2\pi} + \int_{\theta_{sb}}^{2\pi-\theta_{sb}} \int_0^{\rho_2(\theta)} \rho d\rho d\theta\right) H_p$$
$$= \left(R_{sb}^2 \theta_{sb} + \frac{1}{2}\int_{\theta_{sb}}^{2\pi-\theta_{sb}} \rho_2^2(\theta) d\theta\right) H_p, \tag{C12}$$
$$H_{s1} = H_p/2. \tag{C13}$$

For the second part,

$$V_2 = 2\int_{\theta_{st}}^{\theta_{sb}} \int_{R_{sb}}^{\rho_2(\theta)} \int_{z_3(\rho)}^{H_p} \rho dz d\rho d\theta$$
$$= \frac{2H_p}{R_{st} - R_{sb}} \int_{\theta_{st}}^{\theta_{sb}} -\frac{1}{3}\left[\rho_2^3(\theta) - R_{sb}^3\right]$$
$$+ \frac{1}{2} R_{st}\left[\rho_2^2(\theta) - R_{sb}^2\right] d\theta, \tag{C14}$$

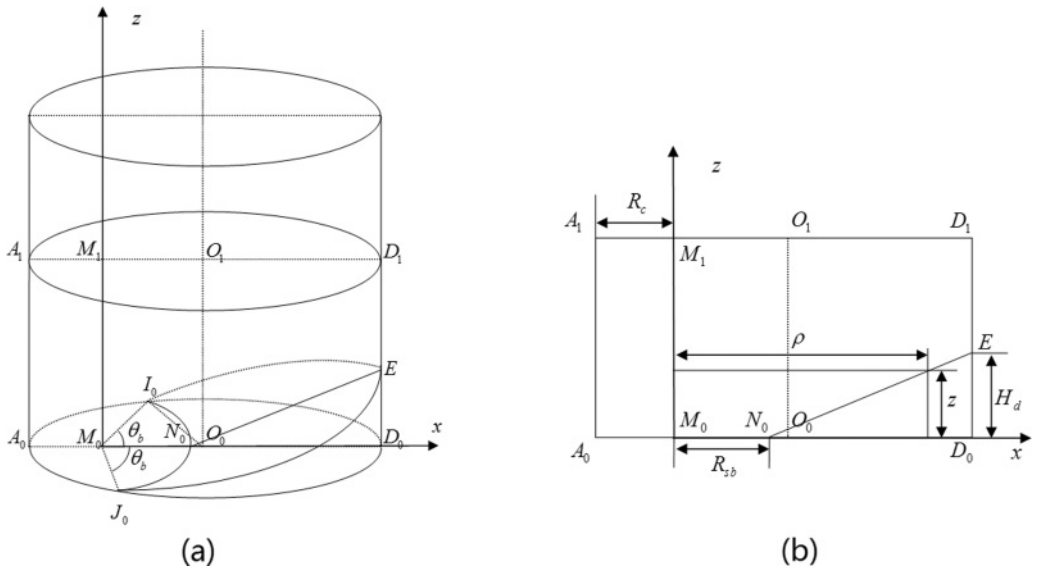

FIG. 14. Illustration of the RBN phase, in which the large particles segregate on one side. The interface remains a conical surface with the axis M_0M_1.

$$H_{s2} = \frac{1}{V_2/2}\int_{\theta_{st}}^{\theta_{sb}}\int_{R_{sb}}^{\rho_2(\theta)}\int_{z_3(\rho)}^{H_p}\rho z\,dz\,d\rho\,d\theta$$
$$= \frac{1}{V_2}\left(\frac{H_p}{R_{st}-R_{sb}}\right)^2\int_{\theta_{st}}^{\theta_{sb}} -\frac{1}{4}\left[\rho_2^4(\theta)-R_{sb}^4\right]$$
$$+\frac{2}{3}R_{sb}\left[\rho_2^3(\theta)-R_{sb}^3\right]$$
$$+\frac{1}{2}\left(R_{st}^2-2R_{sb}R_{st}\right)\left[\rho_2^2(\theta)-R_{sb}^2\right]d\theta. \quad \text{(C15)}$$

For the third part,

$$V_3 = \int_{-\theta_{st}}^{\theta_{st}}\int_{R_{sb}}^{R_{st}}\int_{z_3(\rho)}^{H_p}\rho\,dz\,d\rho\,d\theta$$
$$= \frac{1}{3}H_p\theta_{st}(R_{st}-R_{sb})(2R_{sb}+R_{st}), \quad \text{(C16)}$$
$$H_{s3} = \frac{1}{V_3}\int_{-\theta_{st}}^{\theta_{st}}\int_{R_{sb}}^{R_{st}}\int_{z_3(\rho)}^{H_p}\rho z\,dz\,d\rho\,d\theta$$
$$= \frac{1}{6V_3}H_p^2\theta_{st}(-R_{sb}+R_{st})(5R_{sb}+3R_{st}). \quad \text{(C17)}$$

Through Eqs. (C12), (C14), (C16), and (A13), R_{sb} is determined. H_s is calculated through (A14), in addition to λ in (6).

Notably, the division of the phases on the λ axis, λ_{BN} and λ_{RBN}, can also be calculated using the methods above. For λ_{BN}, we suppose that suppose $H_d = H_p$. For λ_{RBN}, we suppose that $R_c + R_{st} = 2R_0$. Moreover, the values of λ_{BN} and λ_{RBN} are easily determined using numerical methods.

APPENDIX D: CALCULATION METHODS FOR THE RBN PHASE

In the RBN phase, the small particles rise on top and cover all the large particles. The convection of small particles in the RBN phase is rather drastic compared with that in other phases. The interface is still considered a conical surface, and the heap height of the big particles H_d is measured based on the distance from the center of small particles' fountain to the rim R_c. See Fig. 14. The directly measured value is H_d. The value calculated thereafter is R_{sb}.

In this case, we calculated the center mass of the large particles, followed by that of the small ones. In $\Delta M_0 I_0 O_0$, we obtain

$$\theta_b = \arccos\frac{(R_0-R_c)^2+R_{sb}^2-R_0^2}{2R_{sb}(R_0-R_c)}. \quad \text{(D1)}$$

For the conical surface, we derive

$$z_4(\rho) = \frac{H_d}{2R_0-R_c-R_{sb}}(\rho-R_{sb}). \quad \text{(D2)}$$

The volume of the large particles is given by

$$V_l = \int_{-\theta_b}^{\theta_b}\int_{R_{sb}}^{\rho_2(\theta)}\int_0^{z_4(\rho)}\rho\,dz\,d\rho\,d\theta$$
$$= \frac{H_d}{2R_0-R_c-R_{sb}}\int_{-\theta_b}^{\theta_b}\frac{1}{3}\left[\rho_2^3(\theta)-R_{sb}^3\right]$$
$$-\frac{1}{2}R_{sb}\left[\rho_2^2(\theta)-R_{sb}^2\right]d\theta, \quad \text{(D3)}$$
$$H_l = \frac{1}{V_l}\int_{-\theta_b}^{\theta_b}\int_{R_{sb}}^{\rho_2(\theta)}\int_0^{z_4(\rho)}\rho z\,dz\,d\rho\,d\theta$$
$$= \frac{1}{2V_l}\left(\frac{H_d}{2R_0-R_c-R_{sb}}\right)^2\int_{-\theta_b}^{\theta_b}\frac{1}{4}\left[\rho_2^4(\theta)-R_{sb}^4\right]$$
$$-\frac{2}{3}R_{sb}\left[\rho_2^3(\theta)-R_{sb}^3\right]+\frac{1}{2}R_{sb}^2\left[\rho_2^2(\theta)-R_{sb}^2\right]d\theta. \quad \text{(D4)}$$

With (D3), the unknown R_{sb} was determined. Through (D4) and (2), H_s was calculated, and the phase parameter λ was further obtained in (6).

The case in which the large particles cover the bottom layer was not observed in our experiment. Therefore, in this model setting, we ignored such a condition.

[1] A. Rosato, K. J. Strandburg, F. Prinz, and R. H. Swendsen, Phys. Rev. Lett. **58**, 1038 (1987).
[2] T. Shinbrot and F. J. Muzzio, Phys. Rev. Lett. **81**, 4365 (1998).
[3] Z. H. Jiang, K. Q. Lu, M. Y. Hou, W. Chen, and X. J. Chen, Acta Phys. Sin. **52**, 2244 (2003).
[4] D. Blair, I. S. Aranson, G. W. Crabtree, V. Vinokur, L. S. Tsimring, and C. Josserand, Phys. Rev. E **61**, 5600 (2000).
[5] C. Song, P. Wang, and H. A. Makse, Nature (London) **453**, 629 (2008).
[6] T. Y. Wang and T. M. Hong, Phys. Rev. E **78**, 061301 (2008).
[7] J. B. Knight, H. M. Jaeger, and S. R. Nagel, Phys. Rev. Lett. **70**, 3728 (1993).
[8] P. V. Quinn and D. C. Hong, Phys. Rev. E **62**, 8295 (2000).
[9] C. P. Liu, L. Wang, and M. Jia, Chin. J. Process Eng. **9**, 216 (2009).
[10] D. Bi, J. Zhang, B. Chakraborty, and R. P. Behringer, Nature (London) **480**, 355 (2011).
[11] A. P. J. Breu, H.-M. Ensner, C. A. Kruelle, and I. Rehberg, Phys. Rev. Lett. **90**, 014302 (2003).
[12] K. Liffman, K. Muniandy, and M. Rhodes, Granular Matter **3**, 205 (2001).
[13] N. Shishodia and C. R. Wassgren, Phys. Rev. Lett. **87**, 084302 (2001).
[14] N. Burtally, P. J. King, and R. Michael, Granular Matter **5**, 57 (2003).
[15] D. C. Hong, P. V. Quinn, and S. Luding, Phys. Rev. Lett. **86**, 3423 (2001).
[16] Q. F. Shi, X. Q. Yan, M. Y. Hou, X. J. Niu, and K. Q. Lu, Chin. Sci. Bull. **48**, 328 (2003).
[17] Y. Z. Zhao, M. Q. Jiang, and J. Y. Zheng, Acta Phys. Sin. **58**, 1812 (2009).
[18] Q. D. Cai, S. Y. Chen, and X. W. Sheng, Chin. Phys. B **20**, 024502 (2011).
[19] K. M. Aoki and F. Yonezawa, Phys. Rev. A **46**, 6541 (1992).
[20] H. M. Jaeger, S. R. Nagel, and R. P. Bringer, Rev. Mod. Phys. **68**, 1259 (1996).
[21] P. Evesque and J. Rajchenbach, Phys. Rev. Lett. **62**, 44 (1989).
[22] E. Clement, J. Duran, and J. Rajchenbach, Phys. Rev. Lett. **69**, 1189 (1992).
[23] C. P. Liu, L. Wang, X. F. Yue, and S. W. Yin, J. Univ. Sci. Technol. Beijing **31**, 256 (2009).
[24] C. P. Liu, L. Wang, P. Wu, and M. Jia, Phys. Rev. Lett. **104**, 188001 (2010).
[25] M. P. Ciamarra, M. D. De Vizia, A. Fierro, M. Tarzia, A. Coniglio, and M. Nicodemi, Phys. Rev. Lett. **96**, 058001 (2006).
[26] K. Feitosa and N. Menon, Phys. Rev. Lett. **88**, 198301 (2002).
[27] M. Hou, H. Tu, R. Liu, Y. Li, K. Lu, P. Y. Lai, and C. K. Chan, Phys. Rev. Lett. **100**, 068001 (2008).
[28] Y. Fan and K. M. Hill, Phys. Rev. Lett. **106**, 218301 (2011).
[29] A. Qadir, Q. F. Shi, X. W. Liang, and G. Sun, Chin. Phys. B **20**, 024502 (2010).
[30] Y. P. Zhang and L. Wang, J. Univ. Sci. Technol. Beijing **26**, 645 (2004).
[31] J. Bougie and K. Duckert, Phys. Rev. E **83**, 011303 (2011)